Resolving subwavelength objects with a crossed wire mesh superlens operated in backscattering mode

Resolving subwavelength objects with a crossed wire mesh superlens operated in backscattering mode

Mário G Silveirinha[1,4]**, Carla R Medeiros**[2]**, Carlos A Fernandes**[2] **and Jorge R Costa**[2,3]

[1] Department of Electrical Engineering—Instituto de Telecomunicações, University of Coimbra, Portugal
[2] Technical University of Lisbon, Instituto Superior Técnico—Instituto de Telecomunicações, 1049-001 Lisbon, Portugal
[3] Lisbon University Institute (ISCTE-IUL), DCTI, 1049-001 Lisbon, Portugal
E-mail: mario.silveirinha@co.it.pt

Abstract. In this work, we demonstrate that a crossed-wires superlens operated in backscattering mode can resolve targets separated by a subwavelength distance. It is theoretically shown that the effect of the backscattered field on the return loss of a probe antenna is sufficiently strong to allow us to discriminate the targets over a broad range of frequencies. These properties have been experimentally confirmed at microwave frequencies.

[4] Author to whom any correspondence should be addressed.

IOP Institute of Physics ⦿ DEUTSCHE PHYSIKALISCHE GESELLSCHAFT

Contents

1. Introduction

The most salient feature of metamaterials is perhaps their ability to manipulate the near-field, enabling complex operations such as the transport of the near-field to long distances [1]–[3], imaging with subwavelength resolution [1]–[8], tunneling the near-field through narrow apertures [9], the resonant enhancement of reactive fields [6]–[8], and magnification and demagnification in a subwavelength scale [10]–[12]. Many of these ideas are rooted in the excitation of surface plasmon polaritons (SPPs)—electron waves that interact resonantly with the radiation field, and that are characterized by very short guided wavelengths [13]. For planar geometries, the most interesting regime of operation requires that the permittivity of the material is such that $\varepsilon \approx -1$ [6, 7]. Even though several natural materials (e.g. semiconductors and noble metals) may satisfy the condition $\varepsilon \approx -1$ at some frequency in the infrared, optical and ultraviolet ranges, in general in order to obtain an effective plasmonic-type response at some specific frequency, one must resort to metamaterials. In particular, several works have developed the concept of 'spoof' SPPs—guided waves supported by structured metals that mimic to some extent the role of SPPs [14]–[16]. However, the current metamaterial designs have an important drawback: the lattice constant at the frequency where $\varepsilon \approx -1$ is only a few times smaller than the wavelength in free space. This holds back the use of the metamaterials in many of the applications outlined above. Indeed, for example, in subwavelength imaging applications it is well known that the ultimate limit of resolution is determined by the characteristic dimension of the metamaterial [17].

There are, however, other mechanisms for interacting with the near-field beyond relying on the plasmonic response of either metals or semiconductors. For example, recently we showed that a dense metallic mesh of non-connected crossed wires can support guided modes associated with extremely short guided wavelengths and that such guided modes may be resonantly coupled to the near-field, somewhat similar to SPPs [18, 19]. Based on these properties, we have suggested that a thin slab of the metamaterial may behave as a 'superlens' that restores subwavelength features inaccessible with conventional systems [20]. However, fundamentally different from Pendry's superlens [6], the effective index of refraction of the crossed wires superlens is positive and extremely large. Even though such a solution does not correspond, even in ideal circumstances, to a perfect lens, it has important advantages compared to designs based on SPPs. Some of its attractive properties are the broadband non-resonant response, with bandwidths exceeding 25% the central frequency, and the fact that the size of the unit cell is

typically a tiny fraction of the free-space wavelength (e.g. $\lambda_0/50$ and even smaller). This enables restoring the near-field details that otherwise would be smeared out by the propagation in the air regions. These properties have been experimentally verified at microwave frequencies [21]. A related line of research of superlensing at optics—based on slabs with very high permittivity—was also explored in a recent publication [22]. Also in [4], it was demonstrated that a wire grid may behave as a spatial filter and that this enables subwavelength imaging. This is, however, different from the crossed wire lens whose principle of operation is based on the resonant coupling of the near-field to the guided modes of the metamaterial.

Here, we build on our previous works and we study for the first time the operation of the crossed wire lens in backscattering mode, based on the detection of perturbations in the return loss of the radiating antenna. We demonstrate, both theoretically and experimentally, that such a mode of operation makes it possible to resolve objects separated by subwavelength distances over a broad range of frequencies. This paper is organized as follows. In section 2, we explain the principle of operation of the proposed system. In section 3, we develop a simple analytical model that enables modelling the response of the crossed wire lens in the scenario of interest. In section 4, we report the experimental results. Finally, in section 5, the conclusions drawn are presented. In this work, the variation with time of the type $e^{j\omega t}$ is assumed and suppressed.

2. The principle of operation

The principle of operation of the system proposed here is remarkably simple and yet extremely powerful. As demonstrated in our previous works [20, 21], the crossed wire lens (and in general any material with extremely large permittivity [22]) enables collimation of the near field, avoiding lateral (with respect to the lens interface) spreading of the beam. Thus, when the field radiated by a probe antenna interacts with a target behind the lens (figure 1), the backscattered field will be as well collimated on the probe antenna position. Since these interactions take place in the near-field, it is expected that the backscattered field will affect the input impedance of the probe antenna (or equivalently may change its return loss—the S_{11} parameter). Thus, the position of the targets may be determined simply by detecting changes on the return loss of the probe antenna.

The geometry of the system under study is depicted in figure 1. It consists of a metamaterial lens, a probe antenna in front of the lens, and a set of targets behind the lens. For simplicity, it is supposed here that there are exactly two targets behind the lens. Both the antenna and the targets are assumed to have cylindrical shape and to be oriented along the x-direction. Indeed, the crossed wire lens is polarization sensitive, and to ensure proper operation, the electric field must be oriented along the x-direction. The crossed wire lens was described in detail in our previous works [20, 21]. It consists of a double wire medium with lattice constant a. The metallic wires (or strips) lie in planes parallel to the xoz-plane and make an angle of $\pm 45°$ with respect to the $z = 0, L$ interfaces. In particular, wires lying in adjacent planes are perpendicular to one another and are separated by the distance $a/2$, i.e. the wires are non-connected. In figure 1(c), we show a photograph of the assembly of the lens prototype. This prototype is the same as the one reported in [21], and it is formed by a stack of about 300 printed circuit boards. More details will be given in section 4.

It should be noted that even in the absence of the targets, the backscattered field is nonzero, due to the effect of reflections at the lens interface. Thus, the effect of the targets on the probe
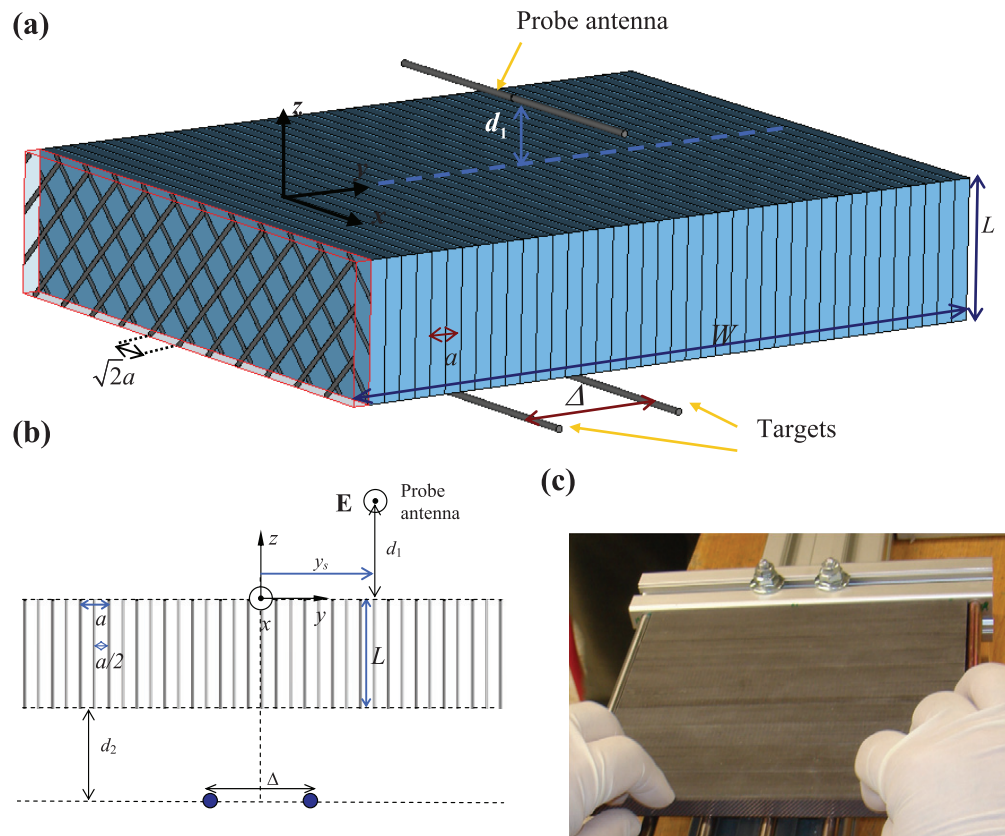
(a)

(b)

(c)

Figure 1. (a) Perspective view of the crossed wire lens, the probe antenna and the targets. (b) Front view of the system. (c) Photograph of the crossed wire lens during the assembly process.

antenna can be characterized by the quantity

$$E_{\mathrm{bs},\delta} = E_{\mathrm{bs}} - E_{\mathrm{bs,lens}}, \tag{1}$$

where E_{bs} is the backscattered field in the presence of lens and targets, and $E_{\mathrm{bs,lens}}$ is the backscattered field in the presence of lens (with no targets). By scanning the probe antenna position (determined by y_s for constant z—see figure 1(b)), it is possible to determine the characteristic $E_{\mathrm{bs},\delta}$ versus y_s. In general, this may involve two different scannings: a calibration scanning without targets ($E_{\mathrm{bs,lens}}$ versus y_s) and a scanning with targets (E_{bs} versus y_s). The peaks of $|E_{\mathrm{bs},\delta}|$ are expected to correspond to the position of the targets.

In section 3, we describe a theoretical model based on effective medium theory that enables one to calculate the backscattered field at the probe antenna position using analytical techniques.

3. The analytical model

For simplicity of modelling, in this section it is assumed that the lens, probe antenna and targets are infinite along the x-direction, so that the problem is two-dimensional (2D) (figure 1(b)). The probe antenna is a line source placed at a distance d_1 above the lens. The coordinate of the line source along the y-direction is y_s. On the other hand, the two targets stand at a distance

d_2 behind the metamaterial slab and are positioned at $y = \pm\Delta/2$, so that the distance between the targets is Δ. Without loss of generality, it is assumed that the targets are metallic and have circular cross-section with radius R. In what follows, we obtain an analytical formula for the backscattered field $E_{\mathrm{bs},\delta}$ as a function of the position of the probe antenna, y_s.

3.1. The total electric field

Our objective is to characterize the effect of the targets on the line source. To this end, we will first calculate the electric field in the air regions. Taking into account that the geometry is 2D, it should be clear that the electric field is oriented along the x-direction: $\mathbf{E} = E_x\hat{\mathbf{x}}$.

It is useful to regard the targets as secondary sources of radiation. Naturally, the field radiated by such secondary sources depends on the probe antenna (line source) and is unknown *a priori*. Using the superposition principle, it is evident that the total electric field is the superposition of the fields $E_{x,i}$ ($i = 1, 2, 3$) created by each individual source (either principal or secondary),

$$E_x = E_{x,1} + E_{x,2} + E_{x,3}, \tag{2}$$

in the presence of the metamaterial lens. Note that within this perspective, the targets (associated with $i = 2, 3$) are being treated on the same footing as the line source ($i = 1$).

It is relatively simple to obtain an explicit expression for $E_{x,i}$. To begin with, we note that the field radiated by a line of current placed at the point $\mathbf{r}_{0,i} = (0, y_{0,i}, z_{0,i})$ in free space is given by

$$E_{x,i}^{\mathrm{rad}} = k_0^2 \frac{p_{\mathrm{e},i}}{\varepsilon_0} \frac{1}{4j} H_0^{(2)}(k_0|\mathbf{r} - \mathbf{r}_{0,i}|) \quad (i = 1, 2, 3), \tag{3}$$

where $k_0 = \omega/c$ is the free-space wave number, $H_0^{(2)}$ is the Hankel function of order zero and second kind, and p_{e} is the electric dipole moment per unit of length (p.u.l.). In the case of the targets ($i = 2, 3$), p_{e} is the induced electric dipole moment, and depends on the polarizability of the scatterers. On the other hand, for an ideal line source (line of electric current), p_{e} is imposed by the external excitation.

The electric field $E_{x,i}$ created by the ith source (which may be either the primary or a secondary source) in the presence of the lens can be readily obtained using Fourier theory. Specifically, $E_{x,i}$ is given by the following Sommerfeld-type integrals

$$E_{x,i}(\mathbf{r}) = \frac{k_0^2 p_{\mathrm{e},i}}{\pi\varepsilon_0} \int_0^\infty \frac{1}{2\gamma_0} e^{-\gamma_0[d(z)+d(z_{0,i})]} T(\omega, k_y) \cos(k_y(y - y_{0,i})) \, \mathrm{d}k_y \tag{4a}$$

if the observation point and the ith source are on different sides of the lens and

$$E_{x,i}(\mathbf{r}) = E_{x,i}^{\mathrm{rad}} + \frac{k_0^2 p_{\mathrm{e},i}}{\pi\varepsilon_0} \int_0^\infty \frac{1}{2\gamma_0} e^{-\gamma_0[d(z)+d(z_{0,i})]} R(\omega, k_y) \cos(k_y(y - y_{0,i})) \, \mathrm{d}k_y \tag{4b}$$

if the observation point and the ith source are on the same side of the lens.

In the above, $R(\omega, k_y)$ and $T(\omega, k_y)$ represent the reflection and transmission coefficients of the metamaterial slab for plane wave incidence with a variation $e^{-jk_y y}$ along the y-direction (for an incident propagating plane wave $k_y = \omega/c \sin\theta_i$, where θ_i is the angle of incidence measured with respect to the normal direction), and $\gamma_0 = \sqrt{k_y^2 - \omega^2/c^2}$. We define $d(z)$ as

the distance between the observation point and the lens interface in the same semi-space, and similarly, $d(z_{0,i})$ is the distance between the ith source and the lens interface in the same semi-space.

Clearly, equation (4) is valid for an arbitrary material slab. The transfer functions $R(\omega, k_y)$ and $T(\omega, k_y)$ completely characterize the slab from the point of view of an observer in the air region. Explicit formulae for $R(\omega, k_y)$ and $T(\omega, k_y)$ have been derived in [20] for the case of a crossed wire metamaterial slab,

$$R(\omega, k_y) = -1 + \cfrac{1}{\begin{aligned}&1 - (k_{z,1}/\gamma_0)[(k_{z,2}^2 + \gamma_h^2)/(k_{z,2}^2 - k_{z,1}^2)]\tan(k_{z,1}(L/2)) \\ &- (k_{z,2}/\gamma_0)[(k_{z,1}^2 + \gamma_h^2)/(k_{z,1}^2 - k_{z,2}^2)]\tan(k_{z,2}(L/2))\end{aligned}} \\ + \cfrac{1}{\begin{aligned}&1 + (k_{z,1}/\gamma_0)[(k_{z,2}^2 + \gamma_h^2)/(k_{z,2}^2 - k_{z,1}^2)]\cot(k_{z,1}(L/2)) \\ &+ (k_{z,2}/\gamma_0)[(k_{z,1}^2 + \gamma_h^2)/(k_{z,1}^2 - k_{z,2}^2)]\cot(k_{z,2}(L/2))\end{aligned}},$$

(5)

$$T(\omega, k_y) = \cfrac{1}{\begin{aligned}&1 - (k_{z,1}/\gamma_0)[(k_{z,2}^2 + \gamma_h^2)/(k_{z,2}^2 - k_{z,1}^2)]\tan(k_{z,1}(L/2)) \\ &- (k_{z,2}/\gamma_0)[(k_{z,1}^2 + \gamma_h^2)/(k_{z,1}^2 - k_{z,2}^2)]\tan(k_{z,2}(L/2))\end{aligned}} \\ - \cfrac{1}{\begin{aligned}&1 + (k_{z,1}/\gamma_0)[(k_{z,2}^2 + \gamma_h^2)/(k_{z,2}^2 - k_{z,1}^2)]\cot(k_{z,1}(L/2)) \\ &+ (k_{z,2}/\gamma_0)[(k_{z,1}^2 + \gamma_h^2)/(k_{z,1}^2 - k_{z,2}^2)]\cot(k_{z,2}(L/2))\end{aligned}}.$$

(6)

In the above, L represents the thickness of the slab, $\gamma_h = \sqrt{k_y^2 - \varepsilon_h \omega^2/c^2}$, ε_h is the relative permittivity of the host dielectric and $k_{z,1} = k_{z,1}(\omega, k_y)$ and $k_{z,2} = k_{z,2}(\omega, k_y)$ are the propagation constants of the modes supported by the metamaterial. The propagation constants $k_{z,1}$ and $k_{z,2}$ can be determined from the effective medium model of the double-wire mesh [18, 20, 23, 24]. Specifically, $k_{z,1}$ and $k_{z,2}$ can be evaluated using equation (3) of [20] (see [20] for more details). It is interesting to mention that the guided modes of the crossed wire medium slab correspond to the poles of the transfer functions $R(\omega, k_y)$ and $T(\omega, k_y)$.

It should be evident that equations (2)–(4) give the total electric field in the air regions written in terms of $p_{e,1}$, $p_{e,2}$ and $p_{e,3}$. As mentioned before, $p_{e,1}$ is determined by the external excitation. The calculation of $p_{e,2}$ and $p_{e,3}$ is addressed next.

3.2. The backscattered field

The dipole moments of the targets ($p_{e,2}$ and $p_{e,3}$) are determined by the local field ($E_{loc,i}$) and the electric polarizability $\alpha_{e,i}$,

$$p_{e,i} = \varepsilon_0 \alpha_{e,i} E_{loc,i} \quad (i = 2, 3).$$

(7)

If the targets are electrically thin metallic wires with radius R and complex permittivity ε, the polarizability $\alpha_{e,i}$ is such that [25]

$$\alpha_e^{-1} = \frac{1}{(\varepsilon - 1)\pi R^2}\left\{1 + (\varepsilon - 1)\frac{(k_0 R)^2}{2}\left[j\frac{\pi}{2} + C + \ln\left(\frac{k_0 R}{2}\right)\right]\right\},$$

(8)

where C is Euler's constant. In particular, for perfect electric conductors (PEC) ($\varepsilon = -\infty$), we have

$$\alpha_e^{-1} = \frac{k_0^2}{2\pi} \left[j\frac{\pi}{2} + C + \ln\left(\frac{k_0 R}{2}\right) \right]. \tag{9}$$

On the other hand, the local field in the vicinity of a given object is the total electric field excluding the self-contribution from the considered object. Hence, the local field on the ith object is given by ($i = 1, 2, 3$)

$$E_{\mathrm{loc},i} = \left[E_{x,i}(\mathbf{r}) - E_{x,i}^{\mathrm{rad}}(\mathbf{r}) \right]\big|_{\mathbf{r}=\mathbf{r}_{0,i}} + \sum_{j \neq i} E_{x,j}(\mathbf{r}_{0,i}). \tag{10}$$

From equation (4), it follows that the local field can be written in terms of the dipoles moments as

$$\begin{bmatrix} E_{\mathrm{loc},1} \\ E_{\mathrm{loc},2} \\ E_{\mathrm{loc},3} \end{bmatrix} = \begin{bmatrix} C_{11} & C_{12} & C_{13} \\ C_{21} & C_{22} & C_{23} \\ C_{31} & C_{32} & C_{33} \end{bmatrix} \begin{bmatrix} p_{e,1}/\varepsilon_0 \\ p_{e,2}/\varepsilon_0 \\ p_{e,3}/\varepsilon_0 \end{bmatrix}, \tag{11}$$

where the interaction constants $C_{i,j}$ are given by

$$C_{i,j} = \frac{k_0^2}{\pi} \int_0^\infty \frac{1}{2\gamma_0} e^{-\gamma_0[d(z_{0,i})+d(z_{0,j})]} T(\omega, k_y) \cos(k_y(y_{0,i} - y_{0,j})) \, \mathrm{d}k_y$$

if $\mathbf{r}_{0,i}$ and $\mathbf{r}_{0,j}$ are on different sides of the lens, \hfill (12a)

and

$$C_{i,j} = k_0^2 \frac{1}{4j} H_0^{(2)}(k_0|\mathbf{r}_{0,i} - \mathbf{r}_{0,j}|) + \frac{k_0^2}{\pi} \int_0^\infty \frac{1}{2\gamma_0} e^{-\gamma_0[d(z_{0,i})+d(z_{0,j})]} R(\omega, k_y) \cos(k_y(y_{0,i} - y_{0,j})) \, \mathrm{d}k_y$$

if $\mathbf{r}_{0,i}$ and $\mathbf{r}_{0,j}$ are on the same side of the lens and if $i \neq j$, and \hfill (12b)

$$C_{i,i} = \frac{k_0^2}{\pi} \int_0^\infty \frac{1}{2\gamma_0} e^{-\gamma_0 2d(z_{0,i})} R(\omega, k_y) \, \mathrm{d}k_y \quad \text{if } i = j. \tag{12c}$$

It can be checked that the matrix of the interaction constants, $[C_{i,j}]$, is symmetric.

Substituting the relations $p_{e,2}/\varepsilon_0 = \alpha_{e,2} E_{\mathrm{loc},2}$ and $p_{e,3}/\varepsilon_0 = \alpha_{e,3} E_{\mathrm{loc},3}$ (which follow from equation (7)) into equation (11), it is possible to determine the local fields $E_{\mathrm{loc},i}$ as a function of the 'external excitation', $p_{e,1}$. This formally solves the problem under study.

Here, we are particularly interested in the backscattered field at the position of the line source. This field describes the influence on the line source of all its surroundings and is evidently given by $E_{\mathrm{bs}} = E_{\mathrm{loc},1}$. After straightforward calculations, it can be proven that when the two targets are identical ($\alpha_e \equiv \alpha_{e,2} = \alpha_{e,3}$), the backscattered field satisfies

$$E_{\mathrm{loc},1} = \left\{ C_{11} + \frac{\alpha_e \left[C_{13}^2(1 - \alpha_e C_{22}) + 2\alpha_e C_{12} C_{13} C_{23} + C_{12}^2(1 - \alpha_e C_{33}) \right]}{1 - \alpha_e(C_{22} + C_{33}) + \alpha_e^2(C_{22}C_{33} - C_{23}^2)} \right\} \frac{p_{e,1}}{\varepsilon_0}. \tag{13}$$

In order to detect the targets, we need to subtract from E_{bs} the backscattered field in the absence of the targets, i.e. $E_{bs,lens}$. It is evident that the latter field can be obtained from equation (13) by setting $\alpha_e = 0$. Hence, we obtain the desired quantity

$$E_{bs,\delta} = \frac{\alpha_e \left[C_{13}^2(1 - \alpha_e C_{22}) + 2\alpha_e C_{12}C_{13}C_{23} + C_{12}^2(1 - \alpha_e C_{33}) \right]}{1 - \alpha_e(C_{22} + C_{33}) + \alpha_e^2(C_{22}C_{33} - C_{23}^2)} \frac{p_{e,1}}{\varepsilon_0}. \tag{14}$$

To conclude this section, we note that the above formula can also be used to determine $E_{bs,\delta}$ in case the metamaterial substrate is absent (i.e. when the targets and the line source stand alone in freespace), provided that in equations (12) we set $R = 0$ and $T = 1$, which corresponds to a slab of zero thickness.

4. Experimental and numerical results

In order to study the potentials of the proposed system, we will first consider a metamaterial lens with the same parameters as the lens of [21]. The thickness of the lens is $L = 11.7\,mm$, the lattice constant is $a = L/7.4$ and the equivalent wire radius is $r_w = 0.05a$. Actually, the prototype reported in [21] is based on a planar design and thus the inclusions are metallic strips rather than round wires. However, to a good approximation a metallic strip with width w_s has an electromagnetic response analogous to a wire with the same cross-sectional perimeter, and thus we can model the prototype of [21] as a metamaterial formed by metallic wires of equivalent radius $r_w = w_s/\pi$. The wires are printed on a dielectric substrate with permittivity $\varepsilon_h = 2.2$.

We assume that the targets are metallic PEC wires with radius $R = 0.5a$. Moreover, it is supposed that the distance between the probe antenna and the lens is the same as the distance between the targets and the lens, and such that $d_1 = d_2 = 0.5L$.

In figure 2, we plot the backscattered field due to the targets, $E_{bs,\delta}$, as a function of the normalized position of the source, y/λ, at different frequencies of operation in the range 1.2–1.7 GHz. The backscattered field is plotted in dB; $|E_{bs,\delta}|_{dB} = 20\log_{10}|E_{bs,\delta}|$, and is normalized to the maximum. The results of figure 2 were obtained using the analytical model (equation (14)). The solid lines in figure 2 represent $|E_{bs,\delta}|_{dB}$ calculated with the metamaterial lens, whereas the dashed lines model the scenario where the lens is removed and the distance between the $z = const$ plane that contains the probe antenna and the plane that contains the targets is reduced to $d = d_1 + d_2$ (i.e. the air thickness remains invariant, while the total distance is reduced to half). We note that at 1.30 GHz the electrical thickness of the lens is about $L = 0.05\lambda$. For each fixed frequency, we consider four different spacings between the targets: $\Delta = 0.4\lambda$, $\Delta = 0.3\lambda$, $\Delta = 0.2\lambda$ and $\Delta = 0.1\lambda$, where λ is the free-space wavelength at the considered frequency.

As seen in figure 2, when the lens is present, notwithstanding the greater distance between the probe antenna and the targets, the resolving properties of the system are dramatically enhanced for target separations down to $\Delta = 0.2\lambda$, for all of the considered frequencies. The best results are achieved around $f \sim 1.20$ GHz, consistent with the fact that the lens of [21] was designed to operate precisely at that frequency. It is also seen in figure 2 that targets separated by $\Delta = 0.1\lambda$ are impossible to discriminate. This property is in agreement with the experimental results of [21], where it was found that the characteristic half-power beamwidth (HPBW) is 0.12λ at 1.24 GHz (and deteriorates for higher frequencies). This value sets the limit of resolution of the lens.
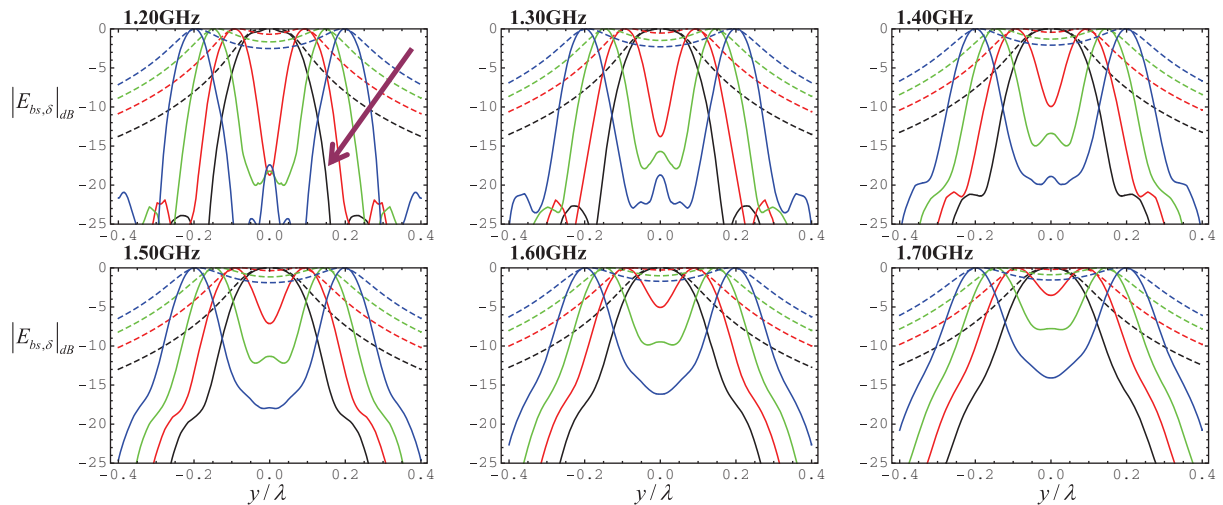
Figure 2. $|E_{\mathrm{bs},\delta}|_{\mathrm{dB}}$ as a function of the position of the probe antenna, y_s/λ, for different target separations: $\Delta = 0.4\lambda_0$ (blue lines), $\Delta = 0.3\lambda_0$ (green lines), $\Delta = 0.2\lambda_0$ (red lines) and $\Delta = 0.1\lambda_0$ (black lines). The solid lines are calculated for the scenario where the lens is present and $d_1 = d_2 = 0.5L$, whereas the dashed lines are calculated for the scenario where the lens is absent and the separation between the scanning plane and the plane that contains the targets is $d = d_1 + d_2 = L$. The arrow in the left upper side plot indicates the direction of decreasing Δ (which is the same in all of the other plots).
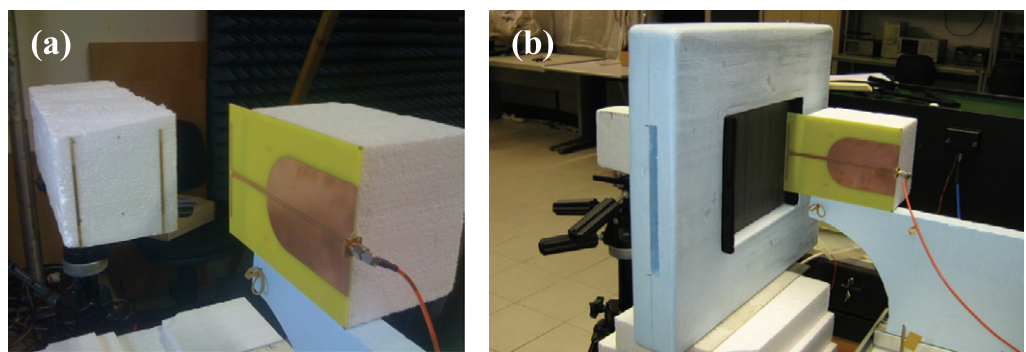

Figure 3. Photographs of the experimental setup. (a) Printed dipole antenna (with a balun) and the two metallic targets. (b) The same setup also showing the metamaterial lens (framed in foam).

As described next, we have experimentally verified the results of the analytical model. The experimental setup is shown in figure 3, and consists of a printed dipole antenna (with a balun) tuned for 1.28 GHz, the metamaterial lens, and two metallic targets. The metamaterial lens prototype has already been reported in [21] (see [21] for more details). The height of the targets is 9.7 cm and the width is $w_{\mathrm{tg}} = 2.5$ mm. To a first approximation, it is possible to obtain $E_{\mathrm{bs},\delta}$ from the perturbations of the return loss of the probe antenna. Specifically, let us define

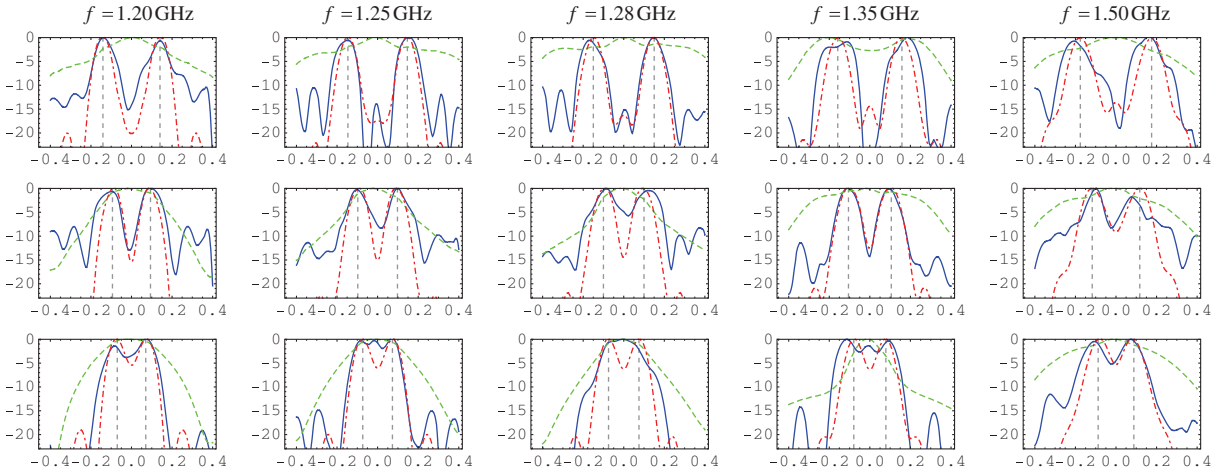$$S_{11,\delta} = S_{11} - S_{11,\mathrm{lens}}, \tag{15}$$

Figure 4. $|S_{11,\delta}|_{dB}$ of the probe antenna as a function of y_s/λ at different frequencies (the frequency is the same for each column of the figure). Solid (blue) lines: measured results with the lens; dashed (green) lines: measured results without the lens; the dot-dashed (red) lines show $|E_{bs,\delta}|_{dB}$ calculated with the theoretical model of section 3 (with the lens). The dashed (gray) vertical lines represent the position of the two objects. The graphics in the first, second and third rows correspond to a spacing between the objects $\Delta = 0.3\lambda_0$, $\Delta = 0.2\lambda_0$ and $\Delta = 0.15\lambda_0$ at 1.28 GHz, respectively (i.e. $\Delta = 7.0\,\text{cm}$, $\Delta = 4.7\,\text{cm}$ and $\Delta = 3.5\,\text{cm}$, respectively).

where S_{11} is the complex valued reflection coefficient at the probe antenna terminals (in the presence of the lens and of the targets), and $S_{11,\text{lens}}$ is the same quantity but when the targets are removed. For a given antenna position, both S_{11} and $S_{11,\text{lens}}$ can be easily measured with the help of a vector network analyzer (VNA). Note that for a lens infinitely extended in the *xoy*-plane, $S_{11,\text{lens}}$ is a constant independent of the position of the antenna (at a fixed source plane). However, for the real finite lens, it is also necessary to determine $S_{11,\text{lens}}$ for each measurement position (y_s). Since to a first approximation the perturbation of the return loss is proportional to the backscattered field, it follows that $S_{11,\delta} \sim E_{bs,\delta}$.

Figure 4 depicts (solid blue lines) the experimentally obtained characteristics $|S_{11,\delta}|_{dB}$ versus y/λ for the target spacings $\Delta = 7.0\,\text{cm}$, $\Delta = 4.7\,\text{cm}$ and $\Delta = 3.5\,\text{cm}$ (first, second and third rows of the figure, respectively). These correspond to $\Delta = 0.3\lambda_0$, $\Delta = 0.2\lambda_0$, and $\Delta = 0.15\lambda_0$ at 1.28 GHz (the resonance frequency of the dipole antenna in free space). By definition, $|S_{11,\delta}|_{dB}$ is $20\log_{10}|S_{11,\delta}|$ normalized to the maximum.

It is seen in figure 4 that for $\Delta = 7.0\,\text{cm}$ and $\Delta = 4.7\,\text{cm}$, the proposed system clearly discriminates the targets. For $\Delta = 3.5\,\text{cm}$, it is still possible to resolve the objects at low frequencies, but already with some difficulty. This is completely consistent with the fact that the limit of resolution is about 0.12λ, as discussed before. For distances inferior to $\Delta = 3.5\,\text{cm}$, our experimental results show that it is impossible to differentiate the targets at low frequencies (not shown).

The dot dashed (red) lines in figure 4 were computed using the theoretical formalism (equation (14)), modeling the targets as round wires with radius $R = w_{tg}/\pi \approx 0.5a$. Despite the many approximations of our analytical model (which assumes a 2D system and that the lens
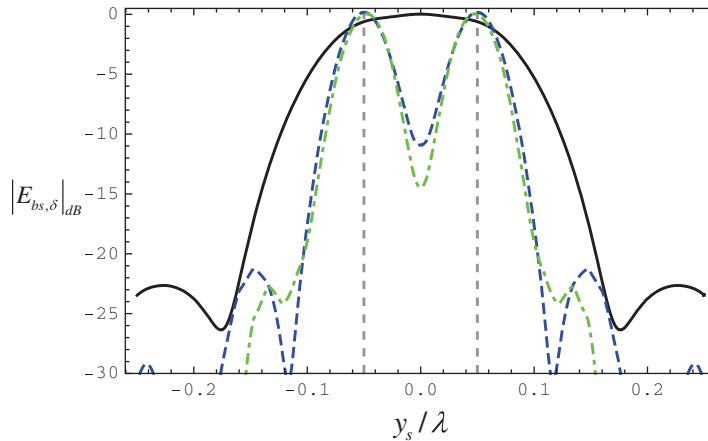
Figure 5. $|E_{\mathrm{bs},\delta}|_{\mathrm{dB}}$ as a function of the position of the probe antenna, y_s/λ, for $\Delta = 0.1\lambda_0$ and $d_1 = d_2 = 0.5L_0$. Solid (black) line: $L = L_0$ and $a = L/7.4$; dashed (blue) line: $L = L_0/6.4$ and $a = L/20$; dot dashed (green) line: $L = L_0/22.9$ and $a = L/40$. The dashed (gray) vertical lines represent the position of the two objects. In all the cases it is assumed that $r_{\mathrm{w}} = 0.05a$.

is infinitely extended in the *xoy*-plane), it clearly captures the physics of the system, and in some cases the general agreement with the measurements is quite remarkable.

Finally, the dashed (green) lines in figure 4 correspond to the experimental results for the scenario where the lens is removed, and the distance between the object and source planes is reduced to $d = d_1 + d_2 = L$. In this case, $S_{11,\delta}$ is defined as $S_{11,\delta} = S_{11} - S_{11,\mathrm{fs}}$, where $S_{11,\mathrm{fs}}$ is the return loss of the antenna in free space. As can be seen, similar to figure 2, without the lens it is impossible to detect the two objects.

We note that in figure 4, some of the plots of the measured characteristics $|S_{11,\delta}|_{\mathrm{dB}}$ versus y/λ are not completely symmetric with respect to $y = 0$. This happens due to some imperfections in the experimental setup as compared to the ideal case. These include the fact that the printed dipole antenna is not completely symmetric with respect to the y-direction (because it is printed on a substrate of finite thickness), the metamaterial lens is not a continuous material and thus the targets may feel its granularity in a different manner, effects of diffraction at the borders of the lens and others.

Even though the resolution of the crossed wire superlens of [21] is about 0.12λ for $d_1 + d_2 \approx 0.05\lambda$, it may be possible to further improve the resolving power of the lens by increasing the density of wires in the metamaterial. In fact, a larger density of wires implies a larger equivalent index of refraction, and this promotes a stronger near-field interaction with spatial harmonics associated with large values of the transverse wave vector, k_y [20].

In order to illustrate this, in figure 5 we depict the characteristics $E_{\mathrm{bs},\delta}$ versus y/λ, calculated with the analytical model at 1.30 GHz for three different metamaterial lenses. The targets are separated by $\Delta = 0.1\lambda$ and are such that $R = 0.79$ mm and $d_1 = d_2 = 0.5L_0$, where $L_0 = 11.7$ mm (as in previous examples). The solid black line of figure 5 corresponds to a metamaterial with $L = L_0$ and $a = L_0/7.4$, i.e. to the parameters of the superlens of [21]. Consistent with figure 2, the targets are not resolved by the system. However, when the density of wires is increased and the lens thickness is fine-tuned, it is possible to resolve the targets (blue and green curves). For example, for $a = L/40$ and $L = L_0/22.9$ (green curve), the objects

are clearly resolved, as the value of $|E_{\mathrm{bs},\delta}|_{\mathrm{dB}}$ at the mid-point is lower than $-14\,\mathrm{dB}$. Note that in all of the examples, the thickness of the air regions $d_1 + d_2$ is kept the same. However, the thickness of the lens differs from case to case. Indeed, as discussed in [20], for a given density of wires (a/L and r_{w}/a fixed) and for a given frequency of operation, the optimal lens thickness L can be obtained by finding the first minimum of the curve T versus L where T is the plane wave transmission coefficient for normal incidence (equation (6) with $k_y = 0$). The lenses of the examples of figure 5 were designed using this procedure, followed by some fine hand tuning. It is also important to mention that unlike in Pendry's lens, in the crossed wire lens, optimal imaging does not necessarily occur when $d_1 = d_2 = 0.5L$, and that there is no general rule regarding the optimal values for d_1 and d_2. In general, the beam is sharper close to the lens interfaces, but only after a minimal distance necessary to ensure the decay of the guided modes supported by the slab.

5. Conclusion

In this work, we have shown both theoretically and experimentally that a material formed by an ultradense array of crossed metallic wires can be operated in backscattering mode and detect targets separated by subwavelength distances. The proposed system has a very broadband response, and is quite insensitive to the effect of metallic loss, as shown by our experimental results and by the theoretical analysis in [20]. A scaled version of our prototype is expected to have a similar performance up to terahertz frequencies [20]. Our system is not based on the excitation of (spoof) SPPs but instead on the extreme effective parameters of the crossed wire mesh [20, 21]. It is interesting to mention that a similar superlensing effect may be obtained with natural materials with a very large index of refraction [22]. In fact, as discussed in [21], our prototype of the metamaterial superlens may have a response somewhat analogous to a dielectric with permittivity $\varepsilon \approx 81$ at the frequencies of interest. However, even when natural materials with low loss and large index of refraction are available, our solution is still interesting because it enables a dramatic enhancement of the electric properties of such materials by using metallic wires as inclusions. It is envisioned that the super-resolving properties of the metamaterial lens may have interesting applications in sensing and radiofrequency identification systems.

Acknowledgments

References

[1] Belov P A, Hao Y and Sudhakaran S 2006 *Phys. Rev.* B **73** 033108
[2] Shvets G, Trendafilov S, Pendry J B and Sarychev A 2007 *Phys. Rev. Lett.* **99** 053903
[3] Silveirinha M G, Belov P A and Simovski C R 2007 *Phys. Rev.* B **75** 035108
[4] Fedorov G, Maslovski S I, Dorofeenko A V, Vinogradov A P, Ryzhikov I A and Tretyakov S A 2006 *Phys. Rev.* B **73** 035409
[5] Freire M J, Marques R and Jelinek L 2008 *Appl. Phys. Lett.* **93** 231108

IOP Institute of Physics ⦶ DEUTSCHE PHYSIKALISCHE GESELLSCHAFT

[6] Pendry J B 2000 *Phys. Rev. Lett.* **85** 3966
[7] Fang N, Lee H, Sun C and Zhang X 2005 *Science* **308** 534
[8] Taubner T, Korobkin D, Urzhumov Y, Shvets G and Hillenbrand R 2006 *Science* **313** 1595
[9] Silveirinha M G and Engheta N 2009 *Phys. Rev. Lett.* **102** 103902
[10] Smolyaninov I I, Hung Y-J and Davis C C 2007 *Science* **315** 1699
[11] Liu Z, Lee H, Xiong Y, Sun C and Zhang X 2007 *Science* **315** 1686
[12] Belov P A, Palikaras G K, Zhao Y, Rahman A, Simovski C R, Hao Y and Parini C 2010 *Appl. Phys. Lett.* **97** 191905
[13] Maier S A 2007 *Plasmonics: Fundamentals and Applications* (New York: Springer)
[14] Pendry J B, Martín-Moreno L and Garcia-Vidal F J 2004 *Science* **305** 6
[15] Williams C R, Andrews S R, Maier S A, Fernández-Dominguéz A I, Martín-Moreno L and García-Vidal F J 2008 *Nat. Photonics* **2** 175–9
[16] Navarro-Cía M, Beruete M, Agrafiotis S, Falcone F, Sorolla M and Maier S 2009 *Opt. Express* **17** 18184
[17] Luo C, Johnson S G, Joannopoulos J D and Pendry J B 2003 *Phys. Rev.* B **68** 045115
[18] Silveirinha M G and Fernandes C A 2008 *Phys. Rev.* B **78** 033108
[19] Silveirinha M G, Fernandes C A, Costa J R and Medeiros C R 2008 *Appl. Phys. Lett.* **93** 174103
[20] Silveirinha M G, Fernandes C A and Costa J R 2008 *Phys. Rev.* B **78** 195121
[21] Silveirinha M G, Medeiros C R, Fernandes C A and Costa J R 2010 *Phys. Rev.* B **81** 033101
[22] Christensen J and García de Abajo F J 2010 *Phys. Rev.* B **82** 161103
[23] Simovski C R and Belov P A 2004 *Phys. Rev.* E **70** 046616
[24] Nefedov I S, Viitanen A J and Tretyakov S A 2005 *Phys. Rev.* E **71** 046612
[25] Silveirinha M G 2006 *Phys. Rev.* E **73** 046612